IOP Publishing Nanotechnology
Nanotechnology **28** (2017) 045704 (10pp) doi:10.1088/1361-6528/28/4/045704

Enhanced peroxidase activity and tumour tissue visualization by cobalt-doped magnetoferritin nanoparticles

Tongwei Zhang[1,2,5], Changqian Cao[1,2,5], Xu Tang[3], Yao Cai[1,2,4], Caiyun Yang[1,2,4] and Yongxin Pan[1,2,3]

[1] Paleomagnetism and Geochronology Laboratory, Key Laboratory of Earth and Planetary Physics, Institute of Geology and Geophysics, Chinese Academy of Sciences, Beijing 100029, People's Republic of China
[2] France-China Bio-Mineralization and Nano-Structures Laboratory, Institute of Geology and Geophysics, Chinese Academy of Sciences, Beijing 100029, People's Republic of China
[3] Electron Microscope Laboratory, Institute of Geology and Geophysics, Chinese Academy of Sciences, Beijing 100029, People's Republic of China
[4] University of Chinese Academy of Sciences, Beijing 100049, People's Republic of China

E-mail: yxpan@mail.iggcas.ac.cn

Received 8 June 2016, revised 21 October 2016
Accepted for publication 1 November 2016
Published 16 December 2016

Abstract

Magnetoferritin (M-HFn) is a biomimetic magnetic nanoparticle with a human heavy-chain ferritin (HFn) shell, trapping a magnetite (Fe_3O_4) core that has inherited peroxidase-like activity. In this study, cobalt-doped M-HFn nanoparticles (M-HFn-$Co_xFe_{3-x}O_4$) with different amounts of cobalt were successfully synthesized. Experimental results indicate that the controlled doping of a certain amount of cobalt into the magnetite cores of M-HFn nanoparticles enhances its peroxidase-like catalytic activity and efficacy for visualizing tumour tissues. For example, compared with sample Co0 (without cobalt doping), the peroxidase-like activity of the cobalt-doped nanoparticle sample Co60 (with a cobalt doping molar percentage of ~34.2%) increases 1.7 times, and has the maximal reaction velocity (V_{max}) values. Moreover, after a one-step incubation with Co60 nanoparticles, and using the peroxidase substrate 3,3′-diaminobenzidine tetrahydrochloride (DAB) for colour development, the tumour tissues of breast, colorectal, stomach and pancreas tumours showed a deeper brown colour with clear boundaries between the healthy and tumourous cells. Therefore, this suggests that the cobalt-doped magnetoferritin nanoparticles enhance peroxidase activity and tumour tissue visualization.

Keywords: magnetoferritin, peroxidase-like activity, kinetic analysis, visualizing tumour tissues, cobalt-doping

(Some figures may appear in colour only in the online journal)

1. Introduction

Magnetic nanoparticles, e.g. Fe_3O_4, possess intrinsic peroxidase-like activity, which is similar to horseradish peroxidase (HRP) [1]. Compared with HRP, the Fe_3O_4 nanoparticles are more stable against denaturation and resistant to high concentrations of substrate [1]. However, conventional synthesized Fe_3O_4 often needs surface modification to prevent aggregation and linking with targeting ligands (such as antibodies, peptides or small molecules), especially for tumour diagnosis [1–4]. Ferritin is an iron storage protein which exists in nearly all organisms. Mature mammalian ferritin is assembled by 24 subunits of heavy-chain (HFn) and light-chain (LFn) ferritin. Natural ferritin forms a cage-like structure with an outer diameter of about 12 nm surrounding an 8 nm cavity containing a core of mineral ferrihydrite [5]. Meldrum *et al* and others successfully replaced the ferrihydrite cores in native horse spleen ferritin with Fe_3O_4 to form

[5] Authors contributed equally to this study.

magnetoferritin (M-HFn) nanoparticles [6–8]. Recently, a novel M-HFn was successfully synthesized through biomimetic mineralization within the recombinant human HFn cavity. The mineralized Fe_3O_4 cores of M-HFn nanoparticles have a uniform shape, narrow size distribution, high crystallinity, monodispersity and superparamagnetism at ambient temperature [9–13]. Importantly, it has been well demonstrated that the M-HFn nanoparticles can be directly used to visualize diverse tumour tissues, because they have the dual functionality of tumour-targeting ability and peroxidase-like activity [12, 14]. Specifically, the HFn shell can specifically target tumours without any surface-targeting ligand modification, and the Fe_3O_4 core exhibits distinct peroxidase-like activity. The H_2O_2 diffuses into the ferritin cavity through its hydrophilic channels and interacts with the iron oxide core of M-HFn to generate ·OH on the surface of the iron core [15]. The generated ·OH catalyze the peroxidase substrate 3,3′-diaminobenzidine tetrahydrochloride (DAB) to produce a colour reaction for visualizing tumour tissues. The dual functionality of M-HFn nanoparticles makes them very appealing in cancer treatment. Recently, the peroxidase-like activity of M-HFn nanoparticles has been demonstrated to be core-size-dependent [8, 12]; M-HFn nanoparticles with larger Fe_3O_4 cores have higher peroxidase-like activity [12]. However, the ferritin cavity strictly controls Fe_3O_4 cores smaller than 8 nm in diameter, so a further increase in the peroxidase-like activity of M-HFn nanoparticles is desired.

Co ions have excellent catalytic activity in H_2O_2 decomposition reactions in place of Fe compounds [16–19]. For example, the Co_3O_4 nanocomposites possess superior peroxidase-like activity than Fe_3O_4 nanoparticles [2, 20]. Fantechi and co-workers recently demonstrated that Co doping of 5% is also enough to enhance hyperthermic efficiency compared with the undoped sample [21]. In the present study, we synthesized and characterized the novel $Co_xFe_{3-x}O_4$ nanocomplex in a HFn cavity to form Co-doped M-HFn nanoparticles (hereafter termed as M-HFn-$Co_xFe_{3-x}O_4$). The systematic peroxidase-like activity kinetics and the tumour-tissue staining efficacy of M-HFn-$Co_xFe_{3-x}O_4$ nanoparticles under different conditions were further analyzed. This indicates that a certain proportion of cobalt doping in the magnetite cores can enhance its peroxidase-like catalytic activity and efficiency for visualizing tumour tissues.

2. Materials and methods

2.1. Recombinant HFn expression and purification

The expression vector, pET-11b, containing the HFn gene, was transformed into *Escherichia coli* BL21 (DE3). The *E. coli* cells were grown at 37 °C to an OD_{600} of 0.8 in an ampicillin-containing liquid Luria-Bertani medium, and induced with isopropyl-β-D-thiogalactopyranoside (IPTG, 1 mM) for 8 h. The cells were harvested by centrifugation at 8 000 rpm for 10 min and the precipitation was washed and re-suspended in Tris-HCl buffer (0.025 M Tris, 0.1 M NaCl, pH 7.4). The suspension was incubated with lysozyme (50 μg ml^{-1}) in the presence of ethylene diaminetetraacetic acid (EDTA, 1 mM) for 1 h at 30 °C, and then heated in the presence of Triton-X 100 (1%) at 75 °C for 20 min. The cells were disrupted and the heat-labile proteins were precipitated. Then the HFn distributed in the supernatant was harvested by centrifugation (10 000 rpm for 30 min at 4 °C), and the purity was analyzed by sodium dodecyl sulfate polyacrylamide gel electrophoresis (SDS-PAGE). The purified HFn was loaded onto a HiPrep 26/20 desalting column (GE Healthcare), and eluted with a 0.1 M NaCl buffer. The concentration of HFn was determined by bicinchoninic acid protein assay reagent (Pierce) with bovine serum albumin as standard.

2.2. Synthesis of M-HFn-$Co_xFe_{3-x}O_4$ nanoparticles

The M-HFn-$Co_xFe_{3-x}O_4$ nanoparticles were synthesized following the previous M-HFn synthesis experimental method with minor modifications [9]. A solution of metal ions (Fe^{2+} and Co^{2+}) was added at a rate of 40 atoms/protein/minute. At the same time, freshly prepared H_2O_2 was added as an oxidant in accordance with stoichiometric equivalents (1:3, H_2O_2: metal ion). Four different proportions of bivalent cobalt-iron solutions were prepared. The starting molar percentage of cobalt (Co/(Co + Fe) × 100) was 0%, 20%, 40%, and 60%, respectively. After adding a theoretical 5 000 atoms per protein cage to the reaction vessel, the reaction continued for another 10 min. Then, 200 μl of 300 mM sodium citrate was added to each sample to chelate any free metal ions. Finally, the purification was performed through size exclusion chromatography (Sepharose 6B, GE Healthcare) after centrifugation at 10 000 rpm for 30 min at 4 °C. These four sets of synthesized M-HFn-$Co_xFe_{3-x}O_4$ nanoparticles were hereafter referred to as Co0, Co20, Co40, and Co60, respectively.

2.3. Characterization of synthesized M-HFn-$Co_xFe_{3-x}O_4$ nanoparticles

The content of iron and cobalt in the M-HFn-$Co_xFe_{3-x}O_4$ nanoparticles was analyzed by inductively coupled plasma mass spectrometry (ICP-MS) (Agilent, 7500 A) according to the experimental procedures described in reference [12]. The samples were nitrified with high-purity hydrogen nitrate at 150 °C in a clean room. The nitrified samples were dissolved in 1 M hydrogen nitrate and quantified to a constant volume of 1 ml. The actual content of metal atoms was calculated by the iron and cobalt standard, respectively.

The size, morphology, and structure of M-HFn-$Co_xFe_{3-x}O_4$ nanoparticles were analyzed by transmission electron microscopy (TEM, JEOL JEM-2100). The samples were dropped onto a carbon-coated copper grid and dried at room temperature. The size distribution of M-HFn-$Co_xFe_{3-x}O_4$ nanoparticles was determined by measuring at least 600 of them. The crystalline of M-HFn-$Co_xFe_{3-x}O_4$ cores was examined by high-resolution TEM (HR-TEM). All images were obtained using an operating beam voltage of 200 kV.

The hysteresis of M-HFn-$Co_xFe_{3-x}O_4$ cores was measured on an MPMS superconducting quantum interference

Table 1. The relevant parameters for the synthesized M-HFn-$Co_xFe_{3-x}O_4$ nanoparticles.

Sample	Co content in starting solution of metal ions (%)	Mean size of cores (nm)	Co content in final nanoparticles (%)	Total atoms per protein (Co ± Fe)	Co stoichiometry (x) in final nanoparticles
Co0	0	5.35 ± 0.95	0	2491	0
Co20	20	5.53 ± 0.94	9.0	2158	0.21
Co40	40	5.54 ± 1.08	17.2	2106	0.52
Co60	60	5.81 ± 0.92	34.2	1969	1.03

device (Quantum Design Inc., Model XP-5XL, with a magnetic moment sensitivity of 5.0×10^{-10} Am^2) in fields of ±3 T at 5 K.

The stability and integrity of the protein shells were examined by circular dichroism (CD) spectra analysis. The CD spectra were obtained using a Chirascan™-Plus CD spectrometer (Applied Photophysics, Leatherhead, UK) at 200–260 nm (bandwidth: 1 nm) with a protein concentration of 0.1 mg ml^{-1}.

2.4. Steady-state kinetic analysis of M-HFn-$Co_xFe_{3-x}O_4$ nanoparticles as peroxidase mimics

Steady-state kinetic assays were performed at room temperature in a 2 ml system with a constant protein concentration of M-HFn-$Co_xFe_{3-x}O_4$ nanoparticles (20 μg ml^{-1}) in a 0.2 M sodium acetate buffer (pH 4.5) in the presence of 100 mM H_2O_2 and 208 μM 3,3,5,5-tetramethylbenzidine (TMB, Sigma). When using H_2O_2 as the substrate, the kinetic analysis was carried out by varying the concentrations of H_2O_2 at a fixed TMB concentration, or vice versa. Colour reactions were recorded immediately after the H_2O_2 was added.

All the reactions were monitored in time scan mode at 652 nm every 4 s during the first 2 min using a UNIC UV/VIS2802 spectrophotometer. The initial reaction velocity was determined by calculating the slope of initial absorbance changes with time. The absorbance data was back-calculated to the concentration by the Beer–Lambert law using a molar absorption coefficient of 39 000 M^{-1} cm^{-1} for the TMB-derived oxidation products [22, 23]. The apparent catalytic parameters were calculated using the Lineweaver–Burk plots of the double reciprocal of the Michaelis–Menten equation, where v is the initial reaction velocity, V_{max} is the maximal reaction velocity, [S] is the substrate concentration, and K_m is the Michaelis constant, which is an indicator of enzyme affinity for its substrate.

$$\text{Michaelis}-\text{Mention equation: } v = (V_{max}[S])/(K_m + [S]) \quad (1)$$

$$\text{Lineweaver}-\text{Burk plots: } 1/v = K_m/(V_{max}[S]) + 1/V_{max} \quad (2)$$

2.5. Staining of tumour tissues using M-HFn-$Co_xFe_{3-x}O_4$ nanoparticles

Frozen xenograft breast tumour (MDA-MB-231) tissue, pancreas tumour (CFPAC-1) tissue, colorectal tumour (HCT-116) tissue and stomach tumour (MGC-803) tissue sections were washed twice in phosphate buffer saline (PBS, pH 7.4) for 3 min and then incubated with 0.3% H_2O_2 in methanol for 20 min to quench endogenous peroxidase activity. For antigen retrieval, the tissue sections were treated with proteinase K for 25 min at 37 °C and washed three times in PBS. The tissue sections were blocked with 5% goat serum in PBS for 1 h at 37 °C, and after washing three times in PBS, independently incubated with Co0 and Co60 nanoparticles (diluted with PBS to 2 μM) overnight at 4 °C. Then, the sections were incubated for an extra 1 h at 37 °C and washed in PBS. Finally, the sections were stained and examined following our previous method with minor modifications [12]. Freshly prepared DAB was used for colour development, while hematoxylin was used for counterstaining. All the sections were dehydrated in anhydrous ethanol and xylene, and eventually mounted with neutral gums. The stained sections were observed under a microscope. Quantitative analysis was carried out using Image Pro Plus software (version 6.0) through calculating the mean optical density, and the intensity was averaged from six fields to view ten tissue sections. First, the MGC-803 tissue was stained with Co60 under pH 4.5, 5.5, 6.5 and 7.5 in order to find out the optimal pH value. Then, the MDA-MB-231, CFPAC-1, and HCT-116 tumour tissues were stained with PBS, Co20 and Co60 at the optimal pH value. The CFPAC-1 tissue staining unfortunately failed as slices were lost during the experiment.

3. Results and discussion

3.1. Mineralogy and magnetism of synthesized M-HFn-$Co_xFe_{3-x}O_4$ nanoparticles

The content of cobalt and the corresponding values of x in the formula unit M-HFn-$Co_xFe_{3-x}O_4$ were calculated and are displayed in table 1. The total iron and cobalt atom content per protein in Co0, Co20, Co40, and Co60 was 2491, 2158, 2106, and 1969 atoms, respectively, while the proportions of cobalt were 0%, 9.0%, 17.2%, and 34.2%, respectively.

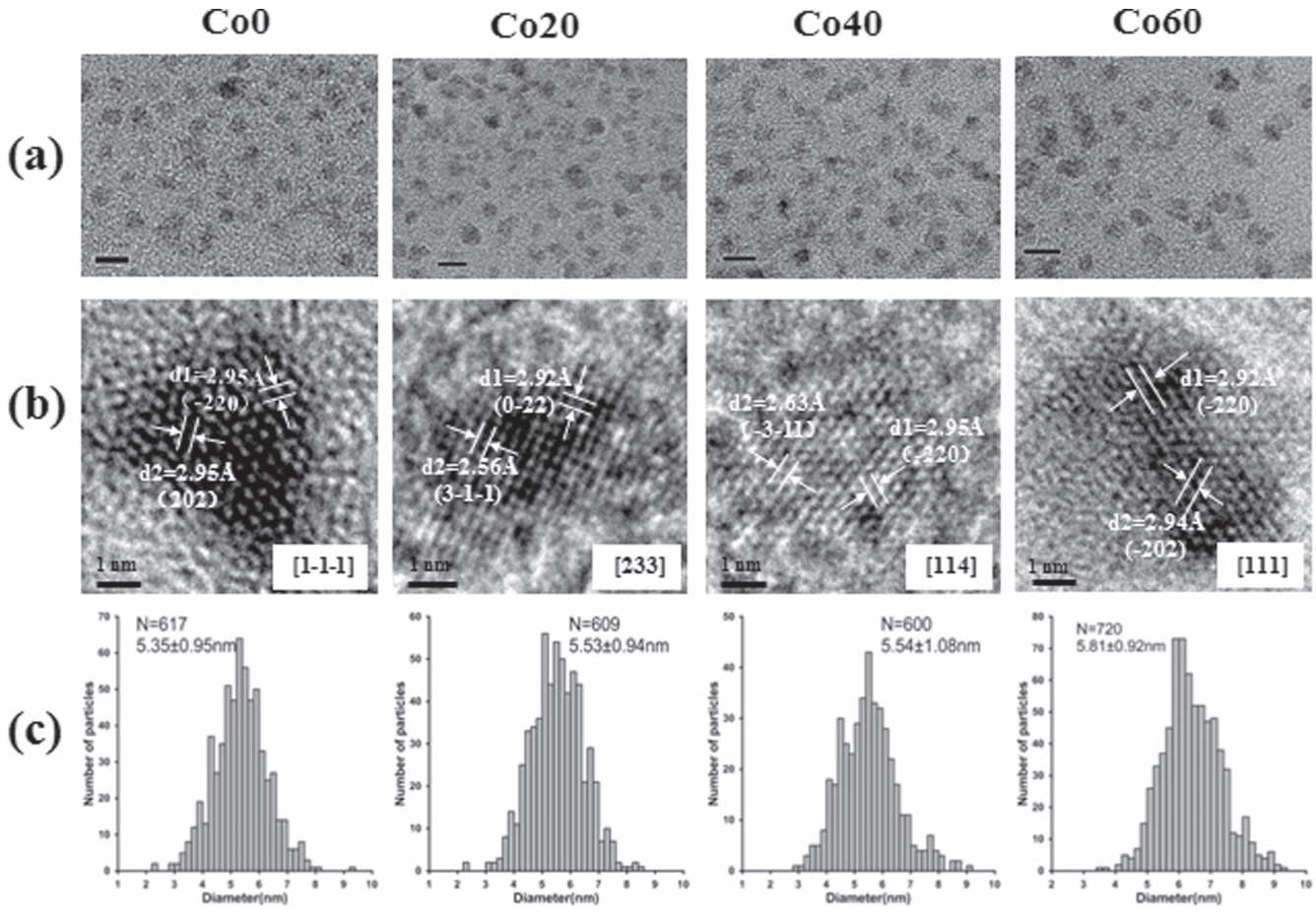

Figure 1. TEM analysis of M-HFn-$Co_xFe_{3-x}O_4$ nanoparticles. (a) TEM graphs of Co0, Co20, Co40, and Co60; scale bar is 10 nm. (b) The HR-TEM images of Co0, Co20, Co40, and Co60; scale bar is 1 nm. (c) Size histograms of Co0, Co20, Co40, and Co60. Abbreviations: M-HFn-$Co_xFe_{3-x}O_4$, magnetic H-ferritin with different rates of cobalt-doping; TEM, transmission electron microscope. Co0, Co20, Co40, and Co60, M-HFn-$Co_xFe_{3-x}O_4$ nanoparticles with starting cobalt proportions of 0%, 20%, 40%, and 60% (by molar percentage), respectively.

As can be seen in figure 1, the synthesized M-HFn-$Co_xFe_{3-x}O_4$ nanoparticles were well monodispersed. The mean size of the cores in Co0, Co20, Co40, and Co60 were 5.35 ± 0.95 nm, 5.53 ± 0.94 nm, 5.54 ± 1.08 nm, and 5.81 ± 0.92 nm, respectively, with shape factors (major axis/minor axis ratios) of 1.05, 1.15, 1.21, and 1.21, respectively. With more cobalt doped into the cores, both the size and shape factor of the cores slightly increased. HR-TEM analysis showed that the cores of all four kinds of samples were well-crystalline with clear lattice fringes (figure 1(b)). However, it was difficult to discriminate between the magnetite and cobalt-doped magnetite during HR-TEM observation due to the similarity between Fe^{2+} and Co^{2+} ions.

Hysteresis loops of the M-HFn-$Co_xFe_{3-x}O_4$ nanoparticles are shown in figures 2(a)–(d). The loop shape, saturation magnetization (M_s) and coercivity (H_c) at 5 K of the M-HFn-$Co_xFe_{3-x}O_4$ nanoparticles varied with cobalt doping. With an increase in the actual content of cobalt doping, the M_s value decreased from 25.0 emu g^{-1} (Co0) to 1.9 emu g^{-1} (Co60) (figure 2(e)). Initially, the H_c value dramatically increased from 20 mT (Co0) to a value of 804 mT (Co20), then decreased to 161 mT (Co60) (figure 2(f)). The observed trends in M_s and H_c are consistent with previous studies [24–28].

3.2. Peroxidase-like activity of M-HFn-$Co_xFe_{3-x}O_4$ nanoparticles

As expected, all four samples Co0, Co20, Co40, and Co60 catalyzed the reaction of the substrates TMB and DAB in the presence of H_2O_2 to produce a blue and brown colour reaction, respectively (figures 3(a) and (b)). These results indicate that M-HFn-$Co_xFe_{3-x}O_4$ nanoparticles exhibit peroxidase-like activity, which is similar to other peroxidase mimetics synthesized by the chemical methods reported previously [2, 29–31]. It is noted that the sample Co60 has about 2.7 times absorbance compared to sample Co0 at 10 min, while the peroxidase-like activity of Co20 and Co40 appear to increase slightly (figure 3).

3.3. Kinetic analysis of M-HFn-$Co_xFe_{3-x}O_4$ nanoparticles as peroxidase mimics

The Michaelis–Menten curves were obtained for the four kinds of M-HFn-$Co_xFe_{3-x}O_4$ nanoparticles with TMB and H_2O_2, respectively, as substrates within the suitable range of concentrations (figures 4(a) and (b)). The K_m and V_{max} were determined by fitting data to the Lineweaver–Burk plot (figures 4(c) and (d)).

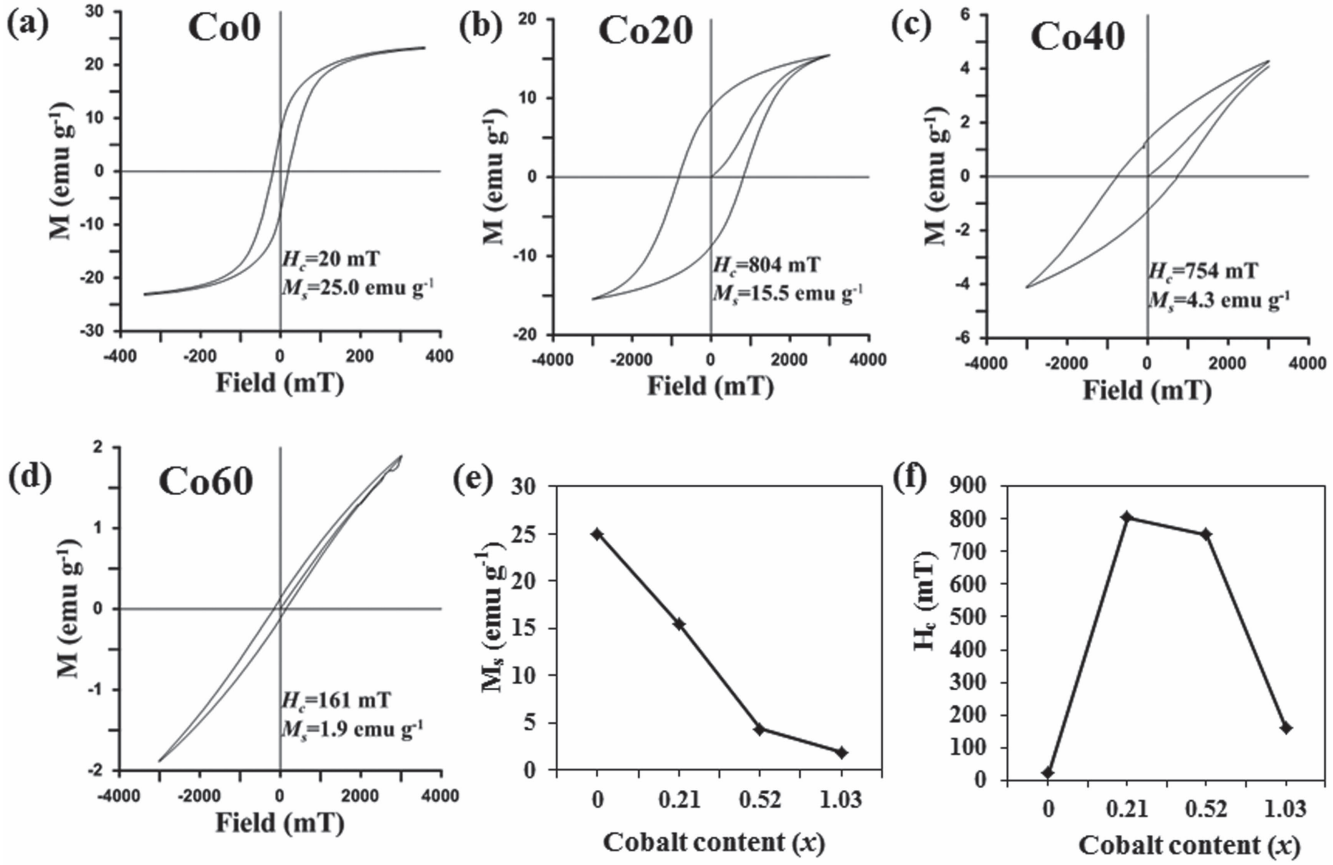

Figure 2. Hysteresis loops of the Co0 (a), Co20 (b), Co40 (c), and Co60 (d) measured at 5 K in fields of ±3 T. The variation of saturation magnetization (e) and coercivity (f) at 5 K as a function of cobalt stoichiometry in M-HFn-$Co_xFe_{3-x}O_4$.

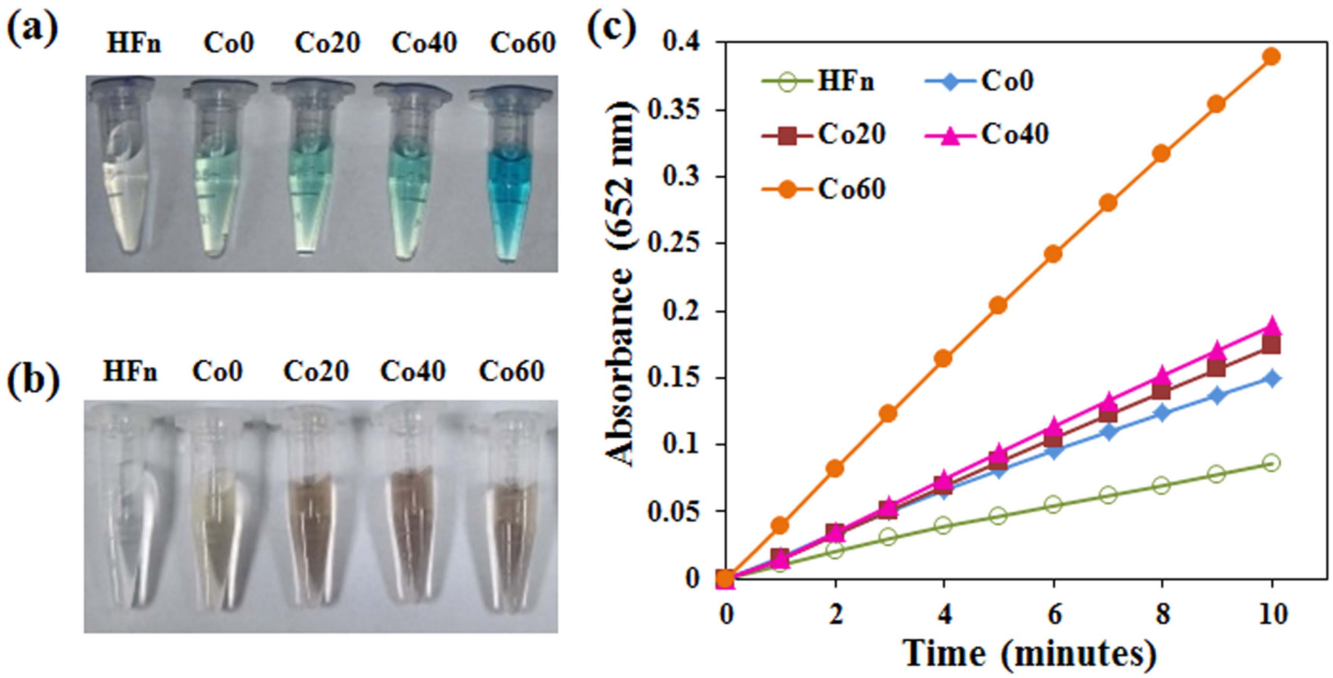

Figure 3. Peroxidase-like activity assays. M-HFn-$Co_xFe_{3-x}O_4$ nanoparticles with different concentrations of cobalt doping catalyzed the oxidation of the peroxidase substrates in the presence of H_2O_2. (a) With TMB, the substrate produced a blue-coloured product. (b) With DAB, the substrate produced a brown-coloured product. (c) A comparison of the peroxidase-like activities of Co0, Co20, Co40, and Co60. The samples contained 100 mM H_2O_2, 208 μM TMB, and 0.2 M sodium acetate buffer (pH 4.5) with the same concentration (20 μg ml^{-1}) of M-HFn-$Co_xFe_{3-x}O_4$ nanoparticles. Pure HFn was tested as a control. The reactions were monitored in time scan mode at 652 nm for 10 min. Abbreviations: HFn, H chain ferritin; TMB, 3,3′,5,5′-tetramethylbenzidine; DAB, 3,3′-diaminobenzidine tetrahydrochloride.

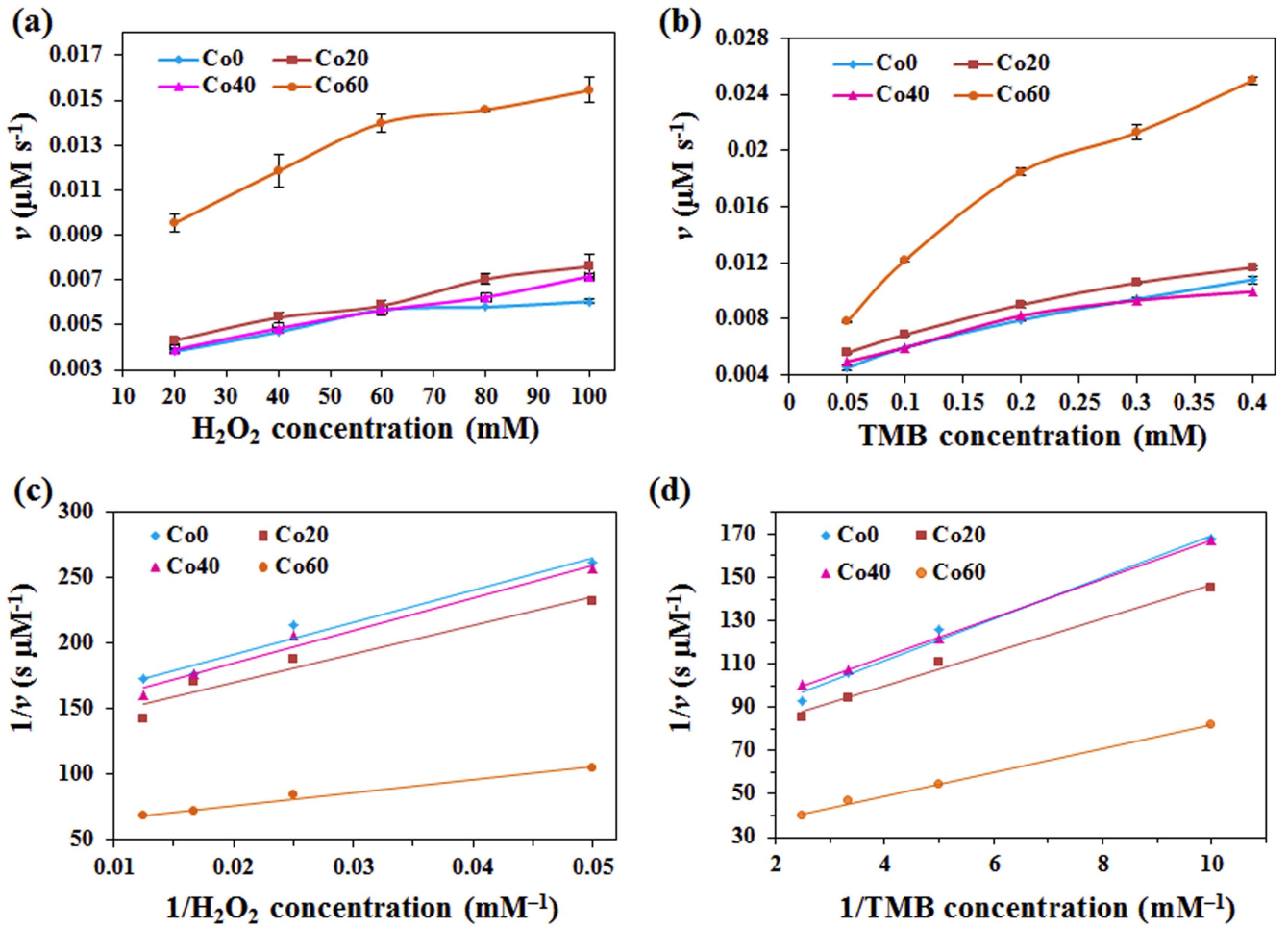

Figure 4. Steady-state kinetic assays of the M-HFn-$Co_xFe_{3-x}O_4$ nanoparticles. (a) The concentration of TMB was 208 μM and the H_2O_2 concentration was varied from 20 mM to 100 mM. (b) The concentration of H_2O_2 was 100 mM and the TMB concentration varied from 0.05 mM to 0.4 mM. (c)–(d) The Lineweaver–Burk plots of the double reciprocal of the Michaelis–Menten equation.

Table 2. The kinetic parameters of the M-HFn-$Co_xFe_{3-x}O_4$ nanoparticles.

Sample	[*E*] (M)	Substrate	K_m(mM)	V_{max} (10^{-9} M s^{-1})
Co0	3.95×10^{-8}	H_2O_2	17.02 ± 3.30	7.01 ± 0.41
Co20	3.95×10^{-8}	H_2O_2	17.17 ± 2.26	7.91 ± 0.34
Co40	3.95×10^{-8}	H_2O_2	18.38 ± 2.58	7.40 ± 0.17
Co60	3.95×10^{-8}	H_2O_2	17.15 ± 2.95	17.57 ± 0.88
Co0	3.95×10^{-8}	TMB	0.13 ± 0.05	13.73 ± 0.31
Co20	3.95×10^{-8}	TMB	0.11 ± 0.02	14.61 ± 1.03
Co40	3.95×10^{-8}	TMB	0.12 ± 0.02	12.92 ± 2.01
Co60	3.95×10^{-8}	TMB	0.20 ± 0.03	36.68 ± 2.84

As shown in figure 4 and table 2, with either H_2O_2 or TMB as the substrate, the K_m values of the M-HFn-$Co_xFe_{3-x}O_4$ nanoparticles were nearly constant in statistical analysis (*t*-test, $P > 0.05$). Specifically, the Co0, Co20, Co40, and Co60 had K_m values of 17.02 ± 3.30 mM, 17.17 ± 2.26 mM, 18.38 ± 2.58 mM, and 17.15 ± 2.95 mM with H_2O_2 as the substrate, and K_m values of 0.13 ± 0.05 mM, 0.11 ± 0.02 mM, 0.12 ± 0.02 mM, and 0.20 ± 0.03 mM with TMB as the substrate, respectively. This suggests that the four kinds of samples have a similar affinity to H_2O_2 as well as TMB. Nevertheless, the Co0, Co20, Co40, and Co60 had V_{max} values of $(7.01 \pm 0.41) \times 10^{-9}$ M s^{-1}, $(7.91 \pm 0.34) \times 10^{-9}$ M s^{-1}, $(7.40 \pm 0.17) \times 10^{-9}$ M s^{-1}, and $(17.58 \pm 0.88) \times 10^{-9}$ M s^{-1} with H_2O_2 as the substrate, and V_{max} values of $(13.73 \pm 0.31) \times 10^{-9}$ M s^{-1}, $(14.61 \pm 1.03) \times 10^{-9}$ M s^{-1}, $(12.92 \pm 2.01) \times 10^{-9}$ M s^{-1}, and $(36.68 \pm 2.84) \times 10^{-9}$ M s^{-1} with TMB as the substrate, respectively (table 2). It is worth noting that at the same molar concentration, the Co60 sample has the highest V_{max} value, while the V_{max} values of Co0, Co20 and Co40

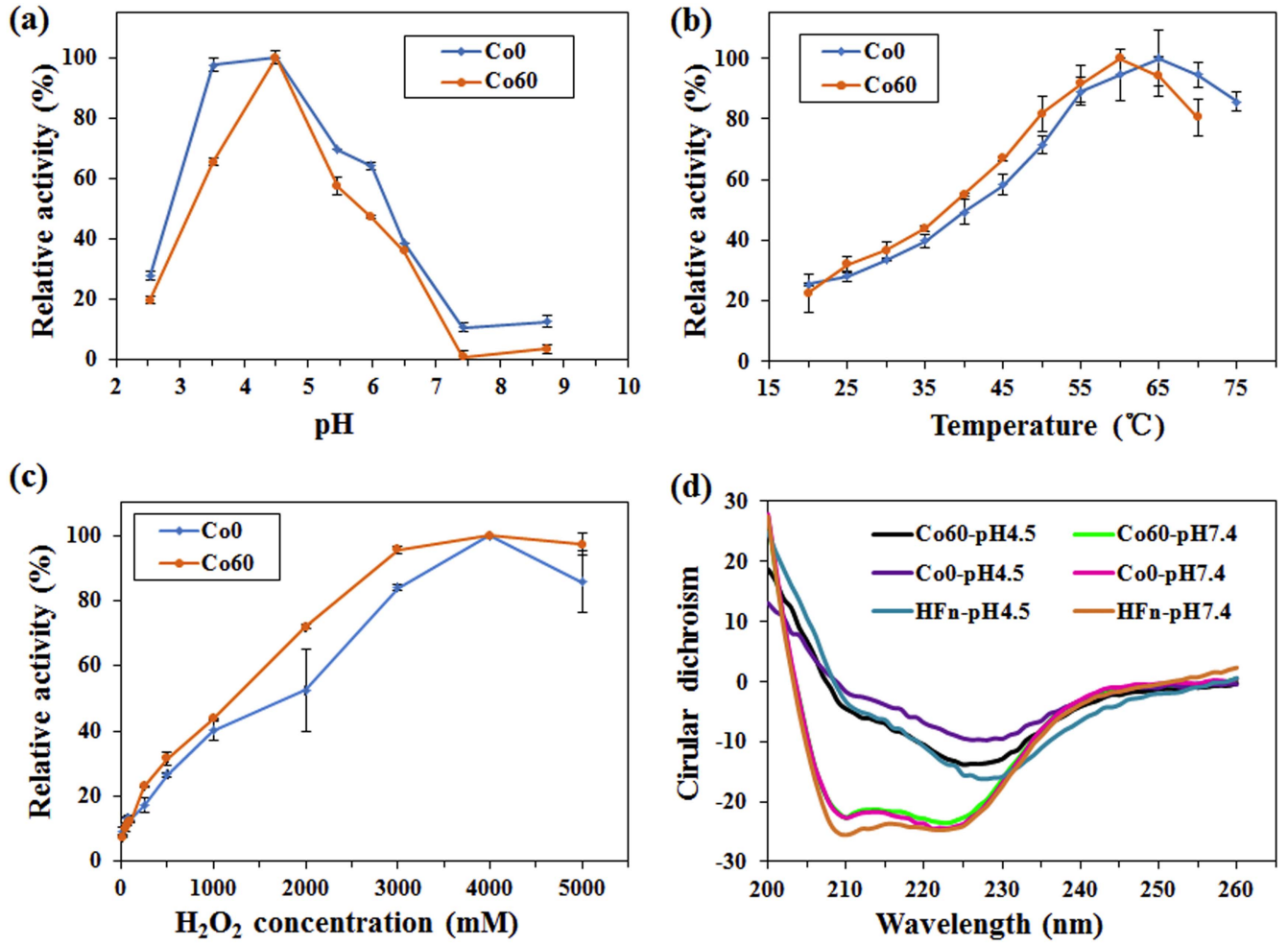

Figure 5. Optimization of catalytic conditions. Experiments were carried out using the same concentration sample Co0 and Co60 with 20 μg protein concentrations in a reaction volume of 2 ml, in a 0.2 M sodium acetate buffer, with 208 μM TMB and 100 mM H_2O_2 as substrates at room temperature. The pH was 4.5, unless otherwise stated. The maximum point in each curve (a)–(c) was set as 100%. (a) Co0 and Co60 showed an optimal pH of 4.5. (b) Co0 and Co60 showed an optimal temperature around 60 °C–65 °C, respectively. (c) Co0 and Co60 required 4 M H_2O_2 to reach maximal peroxidase-like activity. (d) CD spectra of the secondary protein structure of HFn, Co0 and Co60 nanoparticles at pH values of 4.5 and 7.4.

Table 3. Comparison of the optimal experimental conditions of the M-HFn-$Co_xFe_{3-x}O_4$ nanoparticles, HRP and other peroxidase-like artificial enzyme mimics.

Catalyst	Size (nm)	pH	H_2O_2 concentration (M)	Temperature (°C)	Reference
Co0	5.35 ± 0.95	4.5	4	65	This study
Co60	5.81 ± 0.92	4.5	4	60	This study
$ZnFe_2O_4$	200	4.0	0.5	40	[33]
Fe_3O_4 NMPs	300	3.5	0.6	40	[1]
Co_3O_4/rGO	Micron grade	3.5	0.1	30	[20]
HRP	—	4.5	0.01	35	[1]

show no striking difference in statistical analysis (*t*-test, $P > 0.05$).

It has been demonstrated that the TMB can be oxidized directly by Co^{3+}; not by radicals generated from H_2O_2; when Co_3O_4 nanoparticles are used as catalysts. Therefore, the Co_3O_4 nanoparticles possess superior peroxidase-like activity than Fe_3O_4 nanoparticles [2]. In this study, we found that the doping of a certain amount of cobalt can enhance the catalytic activity of M-HFn, and their catalytic activity is cobalt-content-dependent. For peroxidase-like artificial enzyme mimics, metal ions on the surface play a major role in the catalytic reaction [32]. It is assumed that the surface area of the Co20 (9.0% cobalt-doped) and Co40 (17.2% cobalt-doped) may be iron dominant, while the surface of Co60 has more cobalt replacement. Analysis of the cobalt distribution in individual core crystals is nevertheless challenging. In addition to the

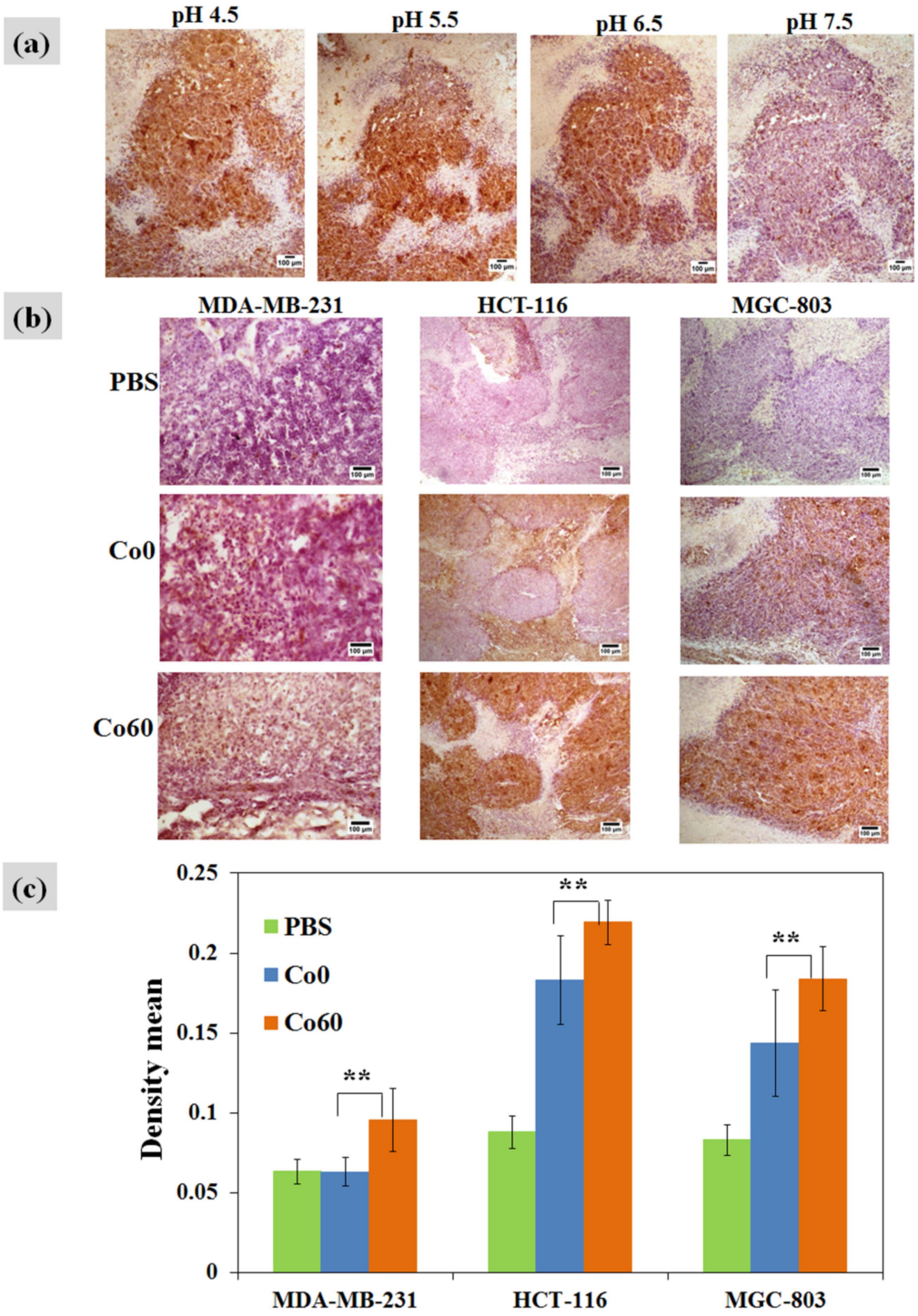

Figure 6. Representative images of the histochemical staining of tumour tissues. (a) Stomach tumour (MGC-803) tissues treated with Co60 and stained in pH 4.5, 5.5, 6.5, and 7.5 conditions; scale bar is 100 μm. (b) Staining of MDA-MB-231 tissue, HCT-116 tissue and MGC-803 tissue with PBS, Co0 and Co60 in pH 6.5 conditions with DAB as the substrate; the scale bar is 100 μm. (c) The mean optical density, showing that treatment with Co60 significantly enhanced the efficiency of histochemical staining. The data was analyzed by *t*-test, and significant differences are indicated by ** ($p < 0.01$).

cobalt doping, the small increase in the core of Co60 (mean size 5.81 ± 0.92 nm) might contribute slightly to the enhancement of peroxidase-like activity.

We also measured the V_{max} of HRP $(1244 \pm 344) \times 10^{-9}$ M s^{-1} with H_2O_2 as the substrate and $(943 \pm 138) \times 10^{-9}$ M s^{-1} with TMB as the substrate. It is noticed that the catalytic activity of M-HFn-$Co_xFe_{3-x}O_4$ nanoparticles is lower than the HRP and some chemically synthesized peroxidase-like artificial enzyme mimics, such as large-sized Fe_3O_4 nanoparticles [1], $CoFe_2O_4$ [30], $ZnFe_2O_4$ [33], $CuFe_2O_4$ [29], Co_3O_4/rGO [20]. However, considering M-HFn nanoparticles have a unique dual functionality of

tumour-targeting ability and peroxidase-like activity, the improvement of catalytic activity by cobalt doping is certainly helpful in tumour detection.

3.4. pH, temperature and H_2O_2 concentration dependence

The pH, temperature and H_2O_2 concentration can influence peroxidase catalytic activity. For example, in neutral or alkaline conditions, H_2O_2 tends to decompose into O_2 and H_2O rather than oxidize the TMB [34]. In this study, the peroxidase-like activities of Co0 and Co60 were studied and compared under different experimental conditions with TMB as the substrate: the pH from 2.53–8.73, the temperature from 20 °C–75 °C, and the H_2O_2 concentration from 0.02–5 M. As shown in figure 5(a), the catalytic activity of both Co0 and Co60 initially increased quickly with the pH up to 4.5, and sharply decreased with further a increase in pH values. Figure 5(b) indicates that the optimal temperature of Co0 and Co60 was slightly different, 65 °C for Co0 and 60 °C for Co60. The effect of H_2O_2 concentration is shown in figure 5(c). Both the Co0 and Co60 required 4 M H_2O_2 to reach the maximal level of peroxidase-like activity. Notably, the temperature and H_2O_2 concentration required to achieve maximal peroxidase-like activity were higher than that of the HRP and some other peroxidase-like artificial enzyme mimics (table 3). A plausible explanation for this is the particle size effect. The high temperature and high H_2O_2 concentration features imply that these M-HFn-$Co_xFe_{3-x}O_4$ nanoparticles could be used in unusual environments.

Figure 5(d) indicates that the CD spectra of Co0 and Co60 at pH 7.4 were very similar to the spectra of HFn, indicative of the native structure of Co0 and Co60 in these conditions. Nevertheless, at pH 4.5, the typical negative peak of the alpha-helix at 208 nm and 222 nm nearly disappeared, which suggests that the secondary structures of HFn, Co0 and Co60 had changed.

3.5. Efficiency of staining tumour tissues

Previous studies have demonstrated that M-HFn nanoparticles can directly target and visualize various tumour tissues including ovarian, liver, prostate, lung, breast, pancreas, cervical, thymus, colorectal and oesophageal cancers. Thanks to the active targeting of the HFn shell to TfR1, the latter is overexpressed in cancer cells [14, 15]. This property makes M-HFn nanoparticles very promising in tumour treatment. In this study, the Co0 (without cobalt doping) and the cobalt-doped Co60 were used in the immunohistochemical-like staining of tumour tissues. Representative images of the histochemical staining of tumour tissues and the mean optical density results are shown in figure 6.

The Co60 staining efficacy at different pH conditions from pH 4.5–7.5 on MGC-803 tissue is shown in figure 6a. It indicates that the tumour tissue staining at pH 4.5–6.5 can distinguish tumours and normal tissues effectively. We selected pH 6.5 as the optimal condition in later staining, because (1) M-HFn nanoparticles have colloidal stability and an intact protein structure between pH 6–10 [14], and (2) because it might cause nonspecific staining due to the structural change of the ferritin shell in pH < 6.0 conditions (see figures 5(d) and 6(a)).

Figures 6(b)–(c) show the staining results with PBS, Co0 and Co60 nanoparticles on MDA-MB-231, HCT-116, and MGC-803 tumour tissues. It demonstrates well that all three tumour tissues treated with Co60 show a significantly more enhanced brown colour than that treated with Co0 and PBS (*t*-test, $p < 0.01$). Our previous staining experiment using Co60 nanoparticles on CFPAC-1 under pH 7.5 also had similar results (data not shown). This indicates that the Co60 nanoparticles possess higher efficiency in the histochemical staining of tumours.

4. Conclusions

We successfully synthesized four kinds of M-HFn-$Co_xFe_{3-x}O_4$ nanoparticles with different amounts of cobalt doping, named Co0, Co20, Co40 and Co60. The catalytic activity of the M-HFn-$Co_xFe_{3-x}O_4$ nanoparticles is dependent on the experimental conditions. The similar K_m values of those M-HFn-$Co_xFe_{3-x}O_4$ nanoparticles infer that the synthesized M-HFn-$Co_xFe_{3-x}O_4$ nanoparticles are equally matched in substrate affinity. In comparison, the Co60 nanoparticles have a maximum V_{max}, exhibiting the strongest peroxidase-like activity, and significantly enhanced staining efficacy of tumour tissues including breast, colorectal, stomach and pancreas tumours.

Acknowledgments

We thank two anonymous reviewers for their very constructive comments that significantly improved the manuscript. This work was supported by CAS Key Research Program of Frontier Sciences, grants from the National Natural Science Foundation of China (41330104, 41574062, 41621004), and the National R&D Projects for Key Scientific Instruments (ZDYZ2012-1-01-02).

References

[1] Gao L, Zhuang J, Nie L, Zhang J, Zhang Y, Gu N, Wang T, Feng J, Yang D and Perrett S 2007 Intrinsic peroxidase-like activity of ferromagnetic nanoparticles *Nat. Nanotechnology* **2** 577–83

[2] Dong J, Song L, Yin J-J, He W, Wu Y, Gu N and Zhang Y 2014 Co_3O_4 nanoparticles with multi-enzyme activities and their application in immunohistochemical assay *ACS Appl. Mater. Interfaces* **6** 1959–70

[3] Liu S, Jia B, Qiao R, Yang Z, Yu Z, Liu Z, Liu K, Shi J, Ouyang H and Wang F 2009 A novel type of dual-modality molecular probe for MR and nuclear imaging of tumor: preparation, characterization and *in vivo* application *Mol. Pharmaceutics* **6** 1074–82

[4] Anzai Y, Blackwell K E, Hirschowitz S L, Rogers J W, Sato Y, Yuh W, Runge V M, Morris M R, McLachlan S J and Lufkin R B 1994 Initial clinical experience with dextran-

coated superparamagnetic iron oxide for detection of lymph node metastases in patients with head and neck cancer *Radiology* **192** 709–15
[5] Theil E C 1987 Ferritin: structure, gene regulation, and cellular function in animals, plants, and microorganisms *Annu. Rev. Biochem.* **56** 289–315
[6] Meldrum F C, Heywood B R and Mann S 1992 Magnetoferritin: *in vitro* synthesis of a novel magnetic protein *Sci.* **257** 522–3
[7] Wong K K, Douglas T, Gider S, Awschalom D D and Mann S 1998 Biomimetic synthesis and characterization of magnetic proteins (magnetoferritin) *Chem. Mater.* **10** 279–85
[8] Melnikova L, Pospiskova K, Mitroova Z, Kopcansky P and Safarik I 2014 Peroxidase-like activity of magnetoferritin *Microchim. Acta* **181** 295–301
[9] Cao C, Tian L, Liu Q, Liu W, Chen G and Pan Y 2010 Magnetic characterization of noninteracting, randomly oriented, nanometer-scale ferrimagnetic particles *J. Geophys. Res.: Solid Earth* **115** B07103
[10] Uchida M, Flenniken M L, Allen M, Willits D A, Crowley B E, Brumfield S, Willis A F, Jackiw L, Jutila M and Young M J 2006 Targeting of cancer cells with ferrimagnetic ferritin cage nanoparticles *J. Am. Chem. Soc.* **128** 16626–33
[11] Uchida M, Terashima M, Cunningham C H, Suzuki Y, Willits D A, Willis A F, Yang P C, Tsao P S, McConnell M V and Young M J 2008 A human ferritin iron oxide nano-composite magnetic resonance contrast agent *Magn. Reson. Med.* **60** 1073–81
[12] Cai Y, Cao C, He X, Yang C, Tian L, Zhu R and Pan Y 2015 Enhanced magnetic resonance imaging and staining of cancer cells using ferrimagnetic H-ferritin nanoparticles with increasing core size *Int. J. Nanomed.* **10** 2619–34
[13] Klem M T, Resnick D A, Gilmore K, Young M, Idzerda Y U and Douglas T 2007 Synthetic control over magnetic moment and exchange bias in all-oxide materials encapsulated within a spherical protein cage *J. Am. Chem. Soc.* **129** 197–201
[14] Cao C, Wang X, Cai Y, Sun L, Tian L, Wu H, He X, Lei H, Liu W and Chen G 2014 Targeted *in vivo* imaging of microscopic tumors with ferritin-based nanoprobes across biological barriers *Adv. Mater.* **26** 2566–71
[15] Fan K, Cao C, Pan Y, Lu D, Yang D, Feng J, Song L, Liang M and Yan X 2012 Magnetoferritin nanoparticles for targeting and visualizing tumour tissues *Nat. Nanotechnology* **7** 459–64
[16] Hanna P M, Kadiiska M B and Mason R P 1992 Oxygen-derived free-radical and active oxygen complex formation from cobalt (II) chelates *in vitro Chem. Res. Toxicology* **5** 109–15
[17] Leonard S, Gannett P M, Rojanasakul Y, Schwegler-Berry D, Castranova V, Vallyathan V and Shi X 1998 Cobalt-mediated generation of reactive oxygen species and its possible mechanism *J. Inorg. Biochem.* **70** 239–44
[18] Verma P, Baldrian P and Nerud F 2003 Decolorization of structurally different synthetic dyes using cobalt (II)/ascorbic acid/hydrogen peroxide system *Chemosphere* **50** 975–9
[19] Kadiiska M B, Maples K R and Mason R P 1989 A comparison of cobalt (II) and iron (II) hydroxyl and superoxide free radical formation *Arch. Biochem. Biophys.* **275** 98–111
[20] Xie J, Cao H, Jiang H, Chen Y, Shi W, Zheng H and Huang Y 2013 Co_3O_4-reduced graphene oxide nanocomposite as an effective peroxidase mimetic and its application in visual biosensing of glucose *Anal. Chim. Acta* **796** 92–100
[21] Fantechi E, Innocenti C, Zanardelli M, Fittipaldi M, Falvo E, Carbo M, Shullani V, Di Cesare Mannelli L, Ghelardini C and Ferretti A M 2014 A smart platform for hyperthermia application in cancer treatment: cobalt-doped ferrite nanoparticles mineralized in human ferritin cages *ACS Nano* **8** 4705–19
[22] Metelitsa D, Savenkova M and Kurchenko V 1987 Optimization of the use of horseradish peroxidase and its antibodies in immunoenzyme analysis *Prikl. Biokhim. Mikrobiologiia* **23** 116–24
[23] Karaseva E, Losev Y P and Metelitsa D 2002 Peroxidase-catalyzed oxidation of 3, 3″, 5, 5″-tetramethylbenzidine in the presence of 2, 4-dinitrosoresorcinol and polydisulfide derivatives of resorcinol and 2, 4-dinitrosoresorcinol *Russ. J. Bioorganic Chem.* **28** 128–35
[24] Carrey J, Mehdaoui B and Respaud M 2011 Simple models for dynamic hysteresis loop calculations of magnetic single-domain nanoparticles: application to magnetic hyperthermia optimization *J. Appl. Phys.* **109** 083921
[25] Sathya A, Guardia P, Brescia R, Silvestri N, Pugliese G, Nitti S, Manna L and Pellegrino T 2016 $Co_xFe_{3-x}O_4$ nanocubes for theranostic applications: effect of cobalt content and particle size *Chem. Mater.* **28** 1769–80
[26] Cullity B D and Graham C D 2009 *Introduction to Magnetic Materials* (Hoboken, NJ: Wiley)
[27] Yu Y, Mendoza-Garcia A, Ning B and Sun S 2013 Cobalt-substituted magnetite nanoparticles and their assembly into ferrimagnetic nanoparticle arrays *Adv. Mater.* **25** 3090–4
[28] Byrne J M, Coker V, Moise S, Wincott P, Vaughan D, Tuna F, Arenholz E, van der Laan G, Pattrick R and Lloyd J 2013 Controlled cobalt doping in biogenic magnetite nanoparticles *J. R. Soc. Interface* **10** 20130134
[29] Hu L, Yuan Y, Zhang L, Zhao J, Majeed S and Xu G 2013 Copper nanoclusters as peroxidase mimetics and their applications to H_2O_2 and glucose detection *Anal. Chim. Acta* **762** 83–6
[30] Shi W, Zhang X, He S and Huang Y 2011 $CoFe_2O_4$ magnetic nanoparticles as a peroxidase mimic mediated chemiluminescence for hydrogen peroxide and glucose *Chem. Commun.* **47** 10785–7
[31] Shi Y, Su P, Wang Y and Yang Y 2014 Fe_3O_4 peroxidase mimetics as a general strategy for the fluorescent detection of H_2O_2-involved systems *Talanta* **130** 259–64
[32] Voinov M A, Pagán J O S, Morrison E, Smirnova T I and Smirnov A I 2010 Surface-mediated production of hydroxyl radicals as a mechanism of iron oxide nanoparticle biotoxicity *J. Am. Chem. Soc.* **133** 35–41
[33] Su L, Feng J, Zhou X, Ren C, Li H and Chen X 2012 Colorimetric detection of urine glucose based $ZnFe_2O_4$ magnetic nanoparticles *Anal. Chem.* **84** 5753–8
[34] Ozgen M, Reese R N, Tulio A Z, Scheerens J C and Miller A R 2006 Modified 2, 2-azino-bis-3-ethylbenzothiazoline-6-sulfonic acid (ABTS) method to measure antioxidant capacity of selected small fruits and comparison to ferric reducing antioxidant power (FRAP) and 2, 2′-diphenyl-1-picrylhydrazyl (DPPH) methods *J. Agric. Food Chem.* **54** 1151–7